CrossMark

RESEARCH PAPER

Effect of Particle Shape on Dilative Behavior and Stress Path Characteristics of Chamkhaleh Sand in Undrained Triaxial Tests

Ali Borhani[1] · Kazem Fakharian[1]

Abstract The behavior of Chamkhaleh sand and three other recognized sands namely, Babolsar, Firouzkuh, and Standard (Ottawa) sands are compared using triaxial apparatus under undrained monotonic loading conditions. Chamkhaleh and Babolsar sands are supplied naturally from southern Caspian Sea shorelines, whereas artificial Firouzkuh and Standard sands were supplied commercially. Samples were prepared using wet tamping with regard to the reduced compaction effect at relative density of 15 % under isotropic consolidation pressures of 100, 300, and 500 kPa. The results of triaxial tests have indicated that Chamkhaleh sand has much more dilation tendency than the other sands. To evaluate the reasons behind this behavior, the sphericity and roundness of all the four sand particles were measured using an image processing method. It was revealed that the sphericity of the four sands is not much different, but Chamkhaleh sand is more angular than the other sands. For comparison of the dilative response of the sands in undrained triaxial tests, a "dilation tendency index" is introduced. This index may be used as a criterion for measuring the dilation of sands in undrained tests. Results have shown that the internal friction angle under the steady-state condition is more dependent on the shape of particles than the maximum strength condition. For sphericities greater than 0.5, the dependency rate of sand behavior on the roundness is decreased.

Keywords Chamkhaleh sand · Undrained triaxial test · Roundness · Sphericity · Dilative

✉ Kazem Fakharian
 kfakhari@aut.ac.ir

[1] Department of Civil and Environmental Engineering, Amirkabir University of Technology, Tehran 15875, Iran

1 Introduction

Most of our understanding of liquefaction phenomena in granular materials has been enlightened through laboratory tests. Liquefaction is observed in monotonic as well as cyclic loading conditions. Under monotonic loading conditions, liquefaction is attributed to the strain-softening behavior [1]. The sand behavior in monotonic and cyclic loading depends on the initial conditions of the specimen, such as relative density, confining pressure, and initial shear stress [2]. The lab studies have also shown that the shape of particles (angularity, sphericity, and surface roughness) has significant effects on the behavior of sands in addition to the initial conditions of the specimen [3]. Most studies conducted on instability of sands in the literature (e.g. [4–11]) indicate that the compressive behavior and likelihood of occurrence of instability under monotonic loading condition increase with a decrease in the relative density and increase in the confining pressure. Hassanlourad et al. [12] compare undrained shear behavior of carbonate and quartz sand. Despite the fact that numerous studies have been carried out on the behavior of sands under various loading conditions, this phenomenon is still receiving the attention of researchers [13].

Terzaghi [14] was the first to show that the shape and size of particles have a great effect on the mechanical behavior of materials. The shape of particles is defined by three criteria, i.e., sphericity, roundness, and surface roughness. The definitions of these three criteria are schematically shown in Fig. 1 [15]. Krumbein and Sloss [16] presented a diagram for estimation of the sphericity and also roundness of particles as shown in Fig. 2. Santamarina and Cho [3] studied the effect of particle shape on the soil behavior. They evaluated the effect of particle shape on various parameters such as strength, deformability, and dynamic properties. Studies have shown that the
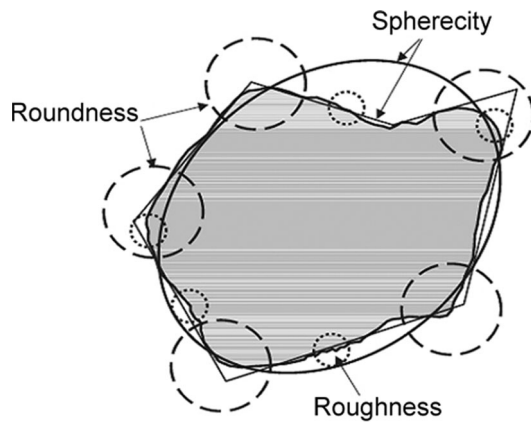
Fig. 1 Schematic definition of sphericity, roundness, and roughness criteria [14]
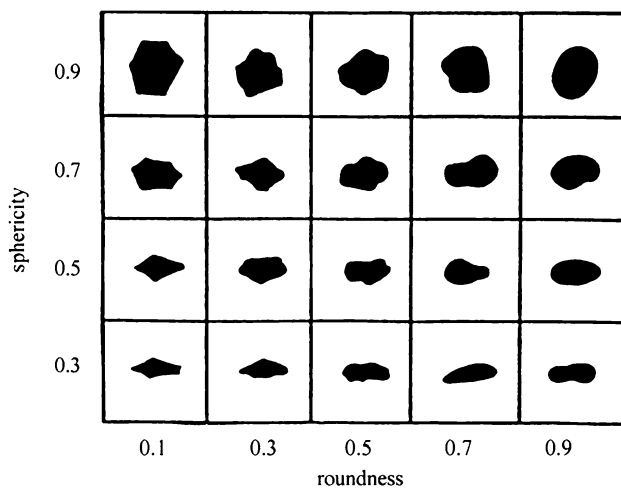

Fig. 2 Schematics of particles with different sphericity and roundness proposed by Krumbein and Sloss [15]

roundness and surface roughness of sands have a significant effect on dilative behavior of sands. The dilation value increases during shearing with decreasing of roundness and increasing of surface roughness. Alshibli and Alsaleh [17], Cho et al. [18], Al-Raoush [19], and Cavarretta [20] were among others who evaluated the effect of particle shape on the behavior of materials.

During the geotechnical investigations operations carried out for the construction of a tourism and entertainment complex in the southern shorelines of the Caspian Sea, a sand type with unusual behavior was observed. In the initial studies, it was revealed that this sand has an unusual great tendency to dilative response [21]. On the other hand, based on the local observations, Chamkhaleh sand liquefied during the Manjil earthquake of 1990. Due to the extraordinary tendency of Chamkhaleh sand to dilative behavior, this sand was classified as an unusual sand [21]. Carbonated sands are another example of unusual sands [22].

The main objective of this paper is to compare the undrained monotonic behavior of Chamkhaleh sand to the three other recognized sands namely Firouzkuh, Babolsar, and Standard (Ottawa) sand [23]. Undrained triaxial tests were carried out on the four sands in loose state and under three confining pressures. Susceptibility to liquefaction depends on the initial state of sand with respect to the steady-state line in e-log p' space; it is not common knowledge that the shape of particles affects the dilative behavior of sand so much that static liquefaction in loose sand in undrained conditions does not occur at all, so sphericity and angularity of all sands are quantified by a specific image processing method. A dilatancy tendency index (DT) is introduced to further evaluate the tendency of dilation of each sand and quantify the shape analyses and interpretations.

2 Materials

The behavior and specifications of Chamkhaleh sand are compared with those of three other recognized sands. The grain size distribution curves are shown in Fig. 3. Babolsar sand is a natural deposit sand supplied from a zone with the same name located adjacent to the Caspian Sea. Firouzkuh is an artificial sand, prepared with various grain sizes, which is widely used in the molding industry. This sand has been widely used in various research studies in Iran [24, 25]. The grain size distribution of Chamkhaleh and Firouzkuh sands is similar. The standard sand and Babolsar sand are also having similar grain size distribution curves. Chamkhaleh sand is the finest, whereas the standard sand is the coarsest of all sands in this study. Specifications of these sands are given in Table 1. Images obtained from microscopic photography are shown in Fig. 4, all having the same size scale.
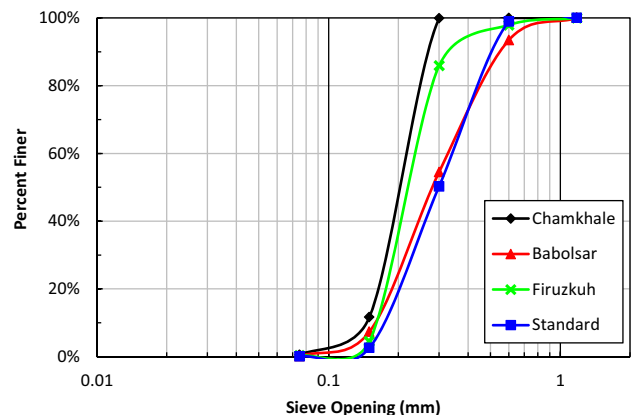

Fig. 3 Grain size distribution of the four sands used in this study

Table 1 Physical properties of the used sands

Sand	D_{50} (mm)	e_{max}	e_{min}	Gs	Cu	Cc
Chamkhale	0.22	0.98	0.68	2.70	1.67	1.02
Babolsar	0.29	0.82	0.54	2.78	2.16	0.91
Firouzkuh (F161)	0.23	0.86	0.58	2.65	1.58	0.96
Standard	0.30	0.69	0.47	2.67	2.08	0.89

Table 2 Mineralogy of the used sands

Sand	Main minerals
Chamkhale	Quartz–Albite–Tridimyte–Sandine
Babolsar	Quartz–Calcite
Firouzkuh (F161)	Quartz
Standard	Quartz
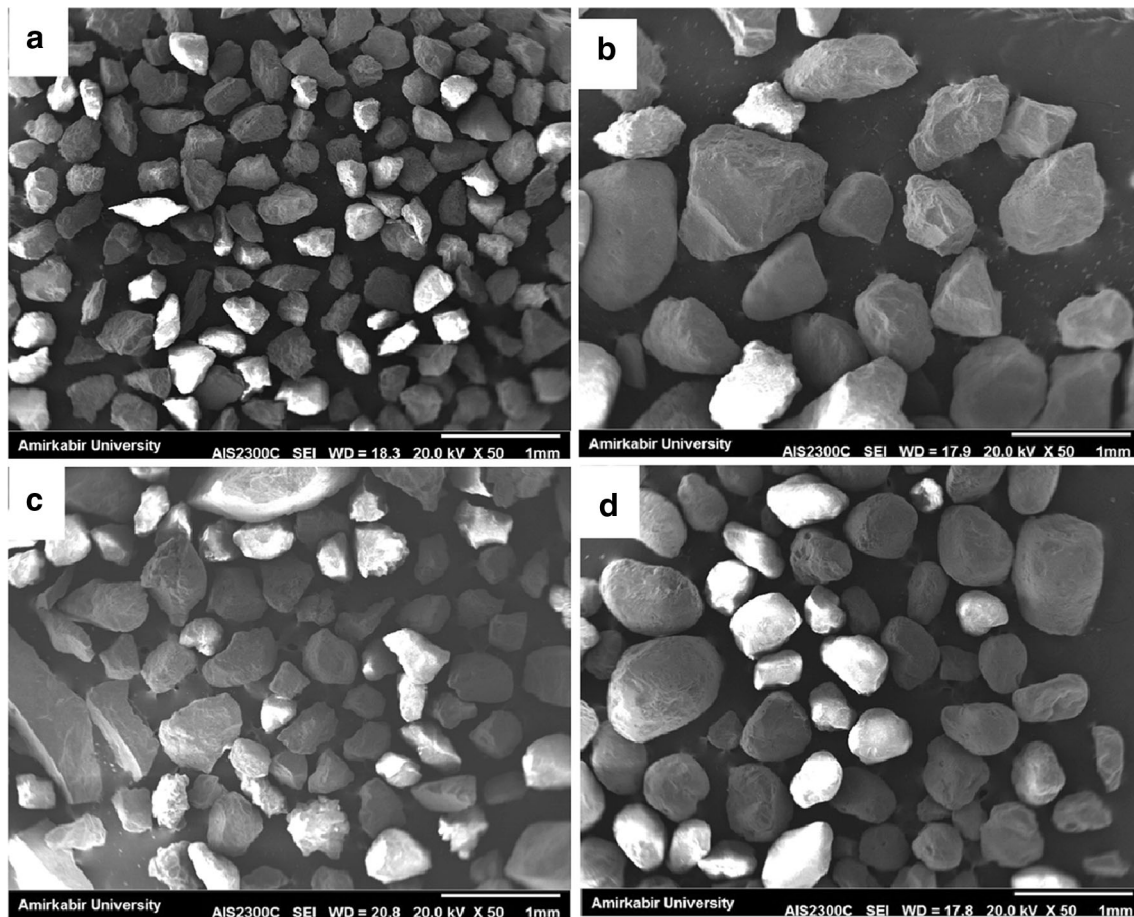
Fig. 4 Microscopic images of sands: **a** Chamkhaleh, **b** Babolsar, **c** Firouzkuh, and **d** Standard (Note: *Scales* are the same for all cases)

The minerals constituting the four sand types were recognized using X-ray imaging method which are shown in Table 2. As it may be seen, quartz is the main mineral constituting all sands. However, low contents of other minerals are seen in Chamkhaleh and Babolsar sands owing to the fact that they are natural deposits.

3 Geology of Chamkhaleh Zone

The Chamkhaleh coastal area is located along the Iranian Caspian coast, adjacent to the eastern boundary of Sefid Rud delta (Fig. 5). From geological point of view, this area is a coastal sedimentary environment [26] covered by Holocene beach deposits including coastal sands (Fig. 5).

The Sefid Rud river is the largest sediment source of the Caspian Sea with 5.2 million tons per year [27], and extends west and northwest of the Chamkhaleh area. During the late Holocene, considerable volumes of sediments were transported to the Caspian Sea by Sefid Rud river. These sediments have then been redistributed by eastward and southeastward long shore currents [28] and accumulated in Chamkhaleh area to form Chamkhaleh delta as shown in Fig. 5.
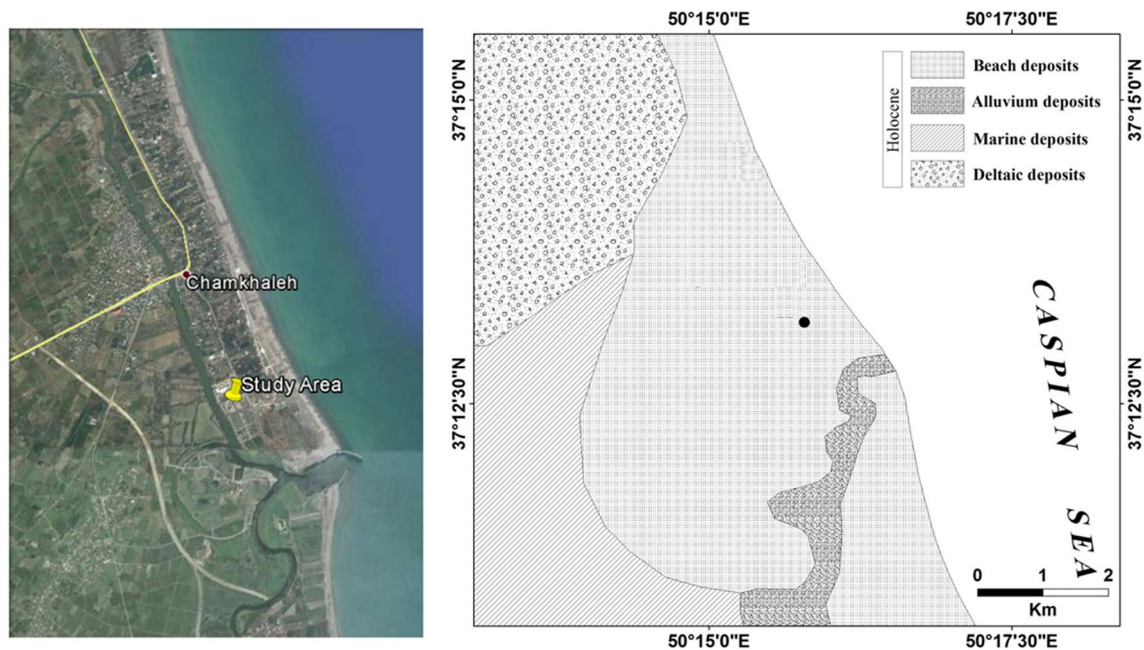
Fig. 5 Location map and geological map of Chamkhaleh coastal area [24]

4 Shape of Particles

Wadell [29] was among the first researchers who came up with a criterion for measuring the shape of particles. After him, Krumbein and Sloss [16] introduced the roundness (R) and sphericity (S) parameters based on Eqs. 1 and 2.

$$R = \frac{(\sum D_i / N)}{D_{\mathrm{max-insc}}} \qquad (1)$$

$$S = \frac{D_{\mathrm{max-insc}}}{D_{\mathrm{max-circ}}} \qquad (2)$$

Definition of each parameter is shown in Fig. 6. Measuring sphericity and roundness based on the proposed equations by Krumbein and Sloss [16] without using the image processing equipment is difficult. Thus, they presented a graph for visual determination of the sphericity and roundness (Fig. 2). In addition to the above-mentioned criteria, various parameters have been given for quantification of the shape of particles. Some of them are mentioned by Masad et al. [30]. Alshibli and Alsaleh [17] proposed two new parameters for measuring the sphericity and roundness of particles.

$$I_{\mathrm{sph}} = \frac{1}{N} \sum_{i=1}^{N} \left| \frac{D_{\mathrm{equ}(i)}}{d_{s(i)}} - \frac{D_{\mathrm{equ}(i)}}{d_{L(i)}} \right| \qquad (3)$$

$$I_R = \frac{1}{N} \sum_{i=1}^{N} \frac{P_{\mathrm{act}(i)}}{\pi \left[(d_{s(i)} + d_{L(i)})/2 \right]} \qquad (4)$$

where, I_{sph} and I_R are sphericity index and roundness index, respectively. d_s and d_L are the smallest and largest diameters of particles, P_{act} is the actual circumference of particles, and D_{equ} is the equivalent particle diameter (the actual circumference divided by Pi number). I_R ranges from 1.0 for well-rounded particles to greater than 1.5 for very angular particles, and I_{sph} ranges from 0.0 for discoidal particles to greater than 1.0 for prismoidal particles.

Considering that separate evaluation of sphericity and roundness effects is not possible in many cases, thus, Choe et al. [18] introduced the average sphericity and roundness, introduced by Krumbein and Sloss [16] as a regularity index (Eq. 5).

$$\rho = \frac{R + S}{2} \qquad (5)$$

Numerical methods have been used for quantifying the shape parameters through image processing methods. Hyslip and Vallejo [31] quantified the shape parameters using the image processing techniques. Bowman et al. [32] demonstrated that if the diagram shown in Fig. 2 was used, the error in estimation of the value of sphericity and roundness would be 0.1 at most, in comparison with other computerized methods. However, the main advantage of image processing methods is their high speed and the capability of evaluating more number of particles, thus a more representative database.

In this study, the image processing toolbox which is provided along with MATLAB software is used to determine the shape parameters. Using this toolbox, the boundary coordination of each particle is determined, and then, mathematical equations and functions are used to
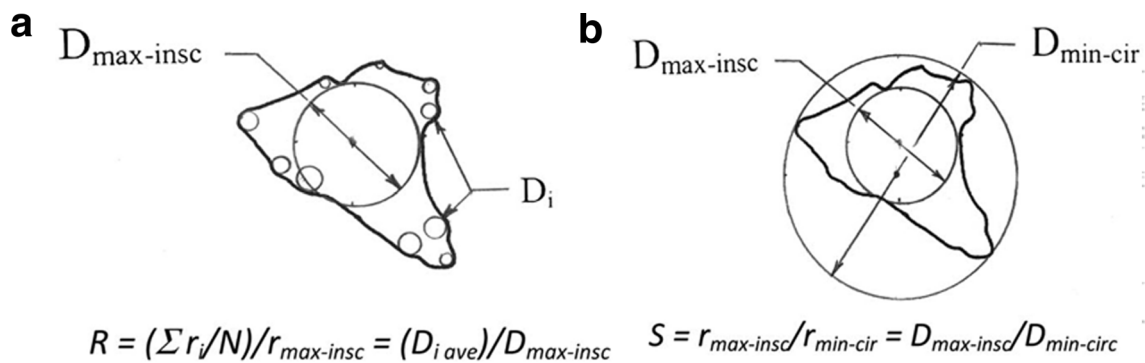
Fig. 6 Krumbein and Sloss procedure for calculation of **a** roundness and **b** sphericity [15]

identify the coordinates of particle corners. Thereafter, inscribed and circumscribed circles and tangent circles are drawn in each corner.

To determine the maximum diameter of the particle circumscribed circle, a number of circles with various center coordinates are plotted using software in such a way to be bounded by the particle, the largest diameter was identified as a circumscribed circle. Similar procedure is used for the inscribed circle, but the circles are plotted from large to small diameter. To plot the tangential circles at the corners, five points were selected adjacent to each corner. The best circle passed through the five points was plotted. If the circle was within the particle domain, it was selected as the tangential circle.

To evaluate the performance of the program, Krumbein and Sloss [16] diagram was primarily used as input, and sphericity and roundness parameters were calculated. The results of this comparison are shown in Fig. 7. The Krumbein and Sloss diagram has proposed five grains with different roundnesses for each sphericity. For example, for sphericity of 0.3, five grains having angularities of 0.1 through 0.9 are introduced, as shown in Fig. 2. This is why the proposed numerical method has ended up in somewhat different sphericities for some of the grains. Figure 7a shows the magnitudes of the computed sphericities corresponding to each roundness. Similar description applies for roundness, as shown in Fig. 7b. As it may be seen, the results of comparison prove to be reasonably good with respect to each other. However, further investigations show that the roundness calculated by software decreases with an increase of sphericity.

Figure 8 shows the methodology used to determine the roundness of one particle for each sand specimen. The image of each grain is shown in the figure before and after image processing. Images a, c, e, and g show four selected grains, for which b, d, f, and h are shown again, respectively, with circles drawn tangent to the corners of each particle. Figure 8i shows one of the grains of Krumbein and Sloss [16] with the image processing method of this study.

The developed program could calculate the sphericity and roundness values reliably. However, when tangent circles are drawn at each corner, some additional corners are also selected other than the principal corners due to digitalization of images. Hence, the plotted circles should be controlled by an operator, and then the additional circles removed. The equations presented by Alshibli and Alsaleh [17] do not require drawing circles. Hence, they could be used in the automated environment more conveniently. Similar to Fig. 7, the sphericity and angularity of diagrams in Fig. 2 using Alshibli and Alsaleh [17] indices (Eqs. 1 and 2) are calculated and compared with the numbers of Krumbein and Sloss [16], as shown in Fig. 9. Alshibli and Alsaleh [17] method predicts sphericity satisfactorily, however, it may not be used to estimate roundness.

According to the suggestions of Choe et al. [18], about 100 particles in the range of average size (d_{50}) for each sand specimen were selected, and an optical microscope with maximum magnification of $40\times$ was used for imaging. Before importing the images into the program, an image editing software was used to convert the images to black and white. Also, in some cases, the particles were located at the edge of the image frame, so the entire particle was not visible. These particles along with the particles that could not be separated due to their contact with each other were excluded from the set of inputs.

The values of sphericity and roundness were calculated for each particle, and the averages were calculated using both arithmetic and geometric methods. No significant differences were observed between the two methods.

Summary of the results is shown in Table 3. As shown in the table, both the sphericity and roundness tend to increase from Chamkhaleh to Babolsar, Firouzkuh, and Standard sands, respectively. Considering the roundness and sphericity of the standard (Ottawa) sand as a base, the roundness of Chamkhaleh, Babolsar, and Firouzkuh, respectively are 76, 61, and 41 % smaller than the standard sand. Similarly, the sphericity of these sands are 14, 9, and 8 % smaller than the standard sand. These numbers are
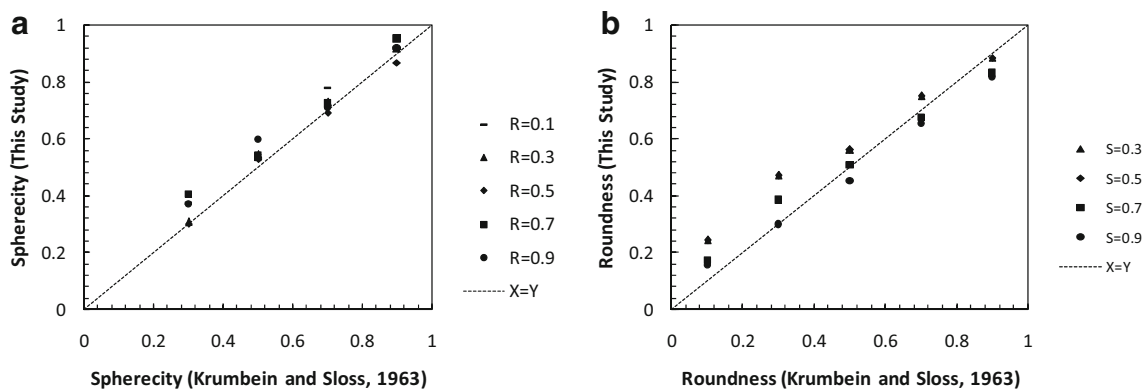
Fig. 7 Comparison of **a** sphericity and **b** roundness obtained from Krumbein and Sloss [15] diagram and image processing techniques of this study
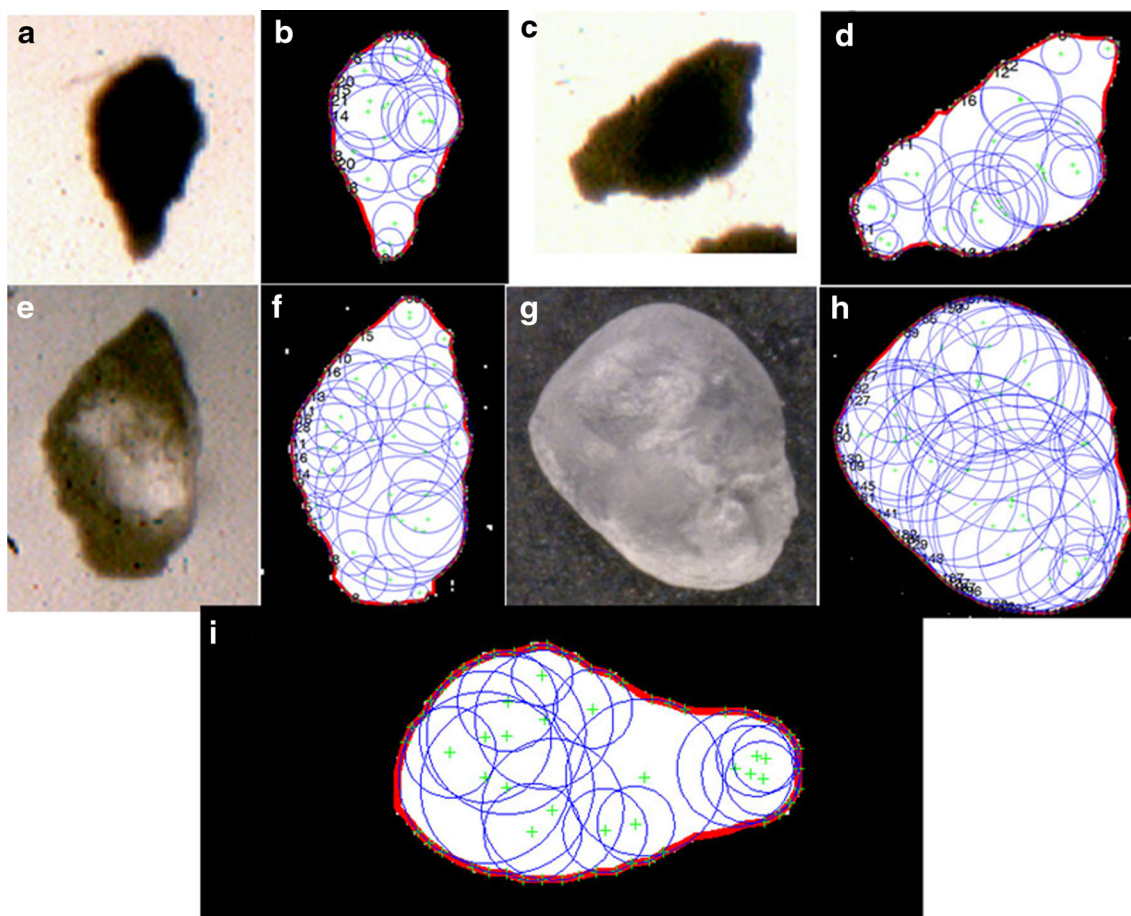

Fig. 8 *Drawing circles* tangent to the corners of each particle. **a**, **b** Chamkhaleh sand, **c**, **d** Babolsar sand, **e**, **f** Firouzkuh sand, and **g**, **h** Standard sand, **i** Krumbein and Sloss [15]

shown in Table 3. The value of regularity index as introduced by Choe et al. [18] is also shown in the table. The differences of regularity index between the three sands and standard sand correspond to the roundness and sphericity indices. Obviously, the differences between roundness of these sands are greater than their sphericity.
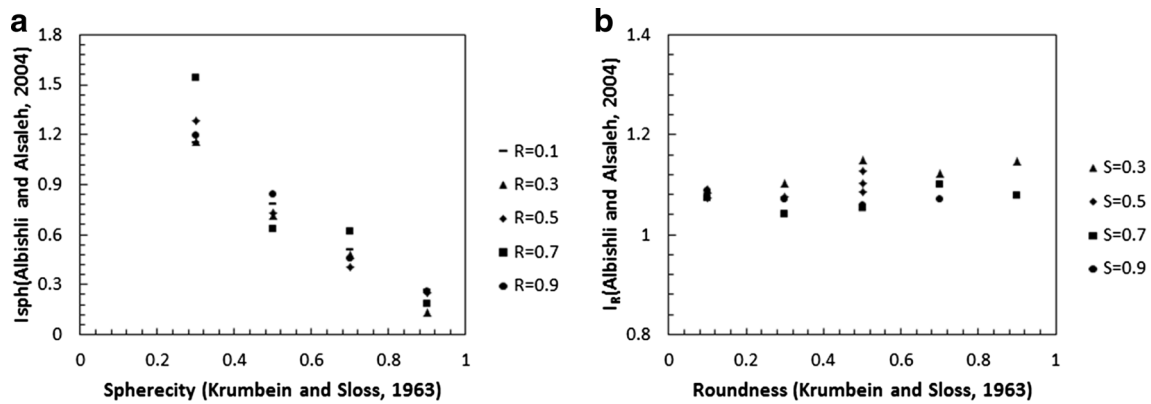
Fig. 9 Comparison of **a** sphericity and **b** roundness obtained from Krumbein and Sloss [15] graph and equations of Alshibli and Alsaleh [16]

Table 3 Summary of the results of sphericity, roundness, and regularity index calculations

	Chamkhale	Babolsar	Firouzkuh	Standard
Roundness				
No. of sample	110	105	98	83
Arithmetic mean	0.212 (76 %)	0.354 (61 %)	0.545 (41 %)	0.919 (0 %)
Geometric mean	0.236	0.330	0.513	0.942
Minimum	0.070	0.176	0.218	0.837
Maximum	0.342	0.415	0.797	0.982
Standard deviation	0.145	0.168	0.279	0.044
Sphericity				
Arithmetic mean	0.698 (14 %)	0.733 (9 %)	0.741 (8 %)	0.807 (0 %)
Geometric mean	0.704	0.721	0.715	0.783
Minimum	0.372	0.389	0.500	0.562
Maximum	0.823	0.903	0.934	0.866
Standard deviation	0.116	0.115	0.099	0.075
Regularity index	0.455 (47 %)	0.543 (37 %)	0.643 (25 %)	0.863 (0 %)

5 Triaxial Compression Tests

Behavior of the four sands with various particle shapes is compared based on monotonic triaxial compression tests. The automated triaxial apparatus of Amirkabir University of Technology with 70-mm diameter specimens was used. All tests were carried out under isotropically consolidated undrained axial compression condition.

Considering the great tendency of Chamkhaleh sand to dilative behavior even at low relative density conditions, all specimens were reconstituted with a relative density of 15 %. Reconstitution of specimens was carried out by wet tamping using under-compaction method as proposed by Ladd [33]. Details of the reconstitution method are presented in Eghbali and Fakharian [25]. After completion of the specimen reconstitution, a confining pressure equal to 20 kPa was applied to the specimen, while CO_2 gas was percolated through the specimen for a duration of 30 min. In the next step, the de-aired water was passed through the specimen. Thereafter, passing water through the specimen

continued until the volume of water reached two times the volume of voids. At the final stage, the saturation operation is followed by subjecting the specimen to back pressure in 50 kPa steps until a Skempton's B parameter [34] of greater than 0.96 at a minimum back pressure of 200 kPa is achieved. The minimum pressure of 200 kPa is applied to prevent the negative pore water pressure effects during the test.

Specimens were consolidated at pressures 100, 300, and 500 kPa. The volume of drained water during the consolidation process along with settlement of the top platen was recorded and used for calculation of relative density at the end of consolidation. Table 4 shows the details of tests. The loading was continued at a rate of 0.53 mm per minute, which is equivalent to a strain rate of 0.33 % per minute, until reaching the maximum axial strain of 20 %. All readings pertaining to the axial forces and displacements, confining pressure, and pore water pressure were recorded automatically during the closed-loop application of the axial compressive load.

Table 4 Details of the monotonic triaxial tests

Test no.	Sand	$(D_r)_0$ (%)	e_0	σ_c (kPa)	$(D_r)_c$ (%)	e_c	B	U_f (%)	DT
1	Chamkhale	15	0.934	100	16.5	0.929	0.96	13	−27
2	Chamkhale	15	0.934	300	17.7	0.926	0.96	6	−10
3	Chamkhale	15	0.934	500	18.5	0.923	0.96	19	−7
4	Babolsar	15	0.778	100	15.7	0.777	0.97	6	−15
5	Babolsar	15	0.778	300	16.5	0.774	0.96	20	6
6	Babolsar	15	0.778	500	17.2	0.772	0.96	42	18
7	Firouzkuh	15	0.818	100	16.3	0.814	0.96	61	13
8	Firouzkuh	15	0.818	300	17.8	0.810	0.96	85	20
9	Firouzkuh	15	0.818	500	18.6	0.808	0.96	90	36
10	Standard	15	0.656	100	16.5	0.653	0.98	73	16
11	Standard	15	0.656	300	18.1	0.650	0.96	94	20
12	Standard	15	0.656	500	19.2	0.647	0.96	98	37

$(D_r)_0$ initial relative density, e_0 initial void ratio, σ_c consolidation pressure, $(D_r)_c$ relative density after consolidation, e_c void ratio after consolidation, B Skempton's B value, U_f flow potential, DT dilation tendency

Cross-section increase of the specimen was considered to calculate the minor and major principal stresses. Lade and Hernandez [35] demonstrated that the membrane penetration effect may be ignored for soils with average grain sizes of 0.2 mm or less. Considering the D_{50} of the sands used (0.29 mm maximum), this correction was not considered.

The diagrams of the deviatoric stress and variations of the pore water pressure with axial strain and also the stress paths in deviatoric stress (q) versus mean effective principal stress (P') space are shown in Fig. 10. As observed in the figure, the Standard sand having the highest sphericity and the lowest angularity has experienced flow liquefaction under all the three consolidation pressures. Similar trend but with lower extent is observed for Firouzkuh sand. The Babolsar sand has experienced flow liquefaction under a consolidation pressure of 500 kPa, while the response has become quite dilative under 100 kPa. An intermediate response is observed for Babolsar sand under a consolidation pressure of 300 kPa. As opposed to all the three other sands, the Chamkhaleh sand has exhibited a clear dilative response under all the three consolidation stresses. The stress–strain relations and stress path plots clearly indicate that except Chamkhaleh sand in which the deviator stress (q) has kept increasing, the strength of other sands has decreased noticeably after the peak strength.

Figure 11 shows the steady-state (SS), maximum strength (Peak), and the phase transformation (PT) lines for all the four sands. The effective internal friction angle was also calculated for the steady-state (ϕ'_{peak}) and maximum strength (ϕ'_{peak}) conditions, and the results are presented in Table 5. It is evident that the SSL and peak strength lines have coincided in Chamkhaleh sand, while the PTL is easily distinguished. In Babolsar sand, the three lines, SSL,

peak strength, and PTL are plotted, showing a slight difference between SSL and peak strength lines. In Firouzkuh and Standard sands, however, only SSL and Peak strength lines could be plotted, as no phase transformation has occurred in the experiments. Table 5 shows that ϕ'_{peak} for the three sands other than Chamkhale are about 1–3 degrees lower than φ'_{SSL}, which is within the observations in the literature for ordinary sands (e.g. [2–7]).

Yoshimine and Ishihara [11] have defined the flow potential as follows:

$$U_f = \left(1 - \frac{p'_{pt}}{p'_c}\right) * 100 \, (\%) \tag{6}$$

Where, U_f is the flow potential, P'_{pt} the mean effective stress at the point of phase transformation, and P'_c is the consolidation stress. The liquefaction potential is calculated for each test, and shown in Table 4. For specimens with no observed specific phase transformation point due to contractive behavior, the final condition point was used for calculation of the liquefaction potential. It is noticed that Chamkhaleh sand has the lowest, and Standard sand has the highest flow potential magnitudes.

The dilation angle parameter in the drained tests is defined as [36]:

$$\psi = \sin^{-1}\left[\frac{-d\varepsilon_v}{d\gamma}\right]. \tag{7}$$

Vaid and Sasitharan [37] rewrote the equation above for drained triaxial compression tests. In this equation, the dilation angle is a function of the volumetric strain to axial strain ratio. The negative sign denotes the tendency to dilation.

In this paper, undrained triaxial tests are performed. However, given that variations in the pore water pressure
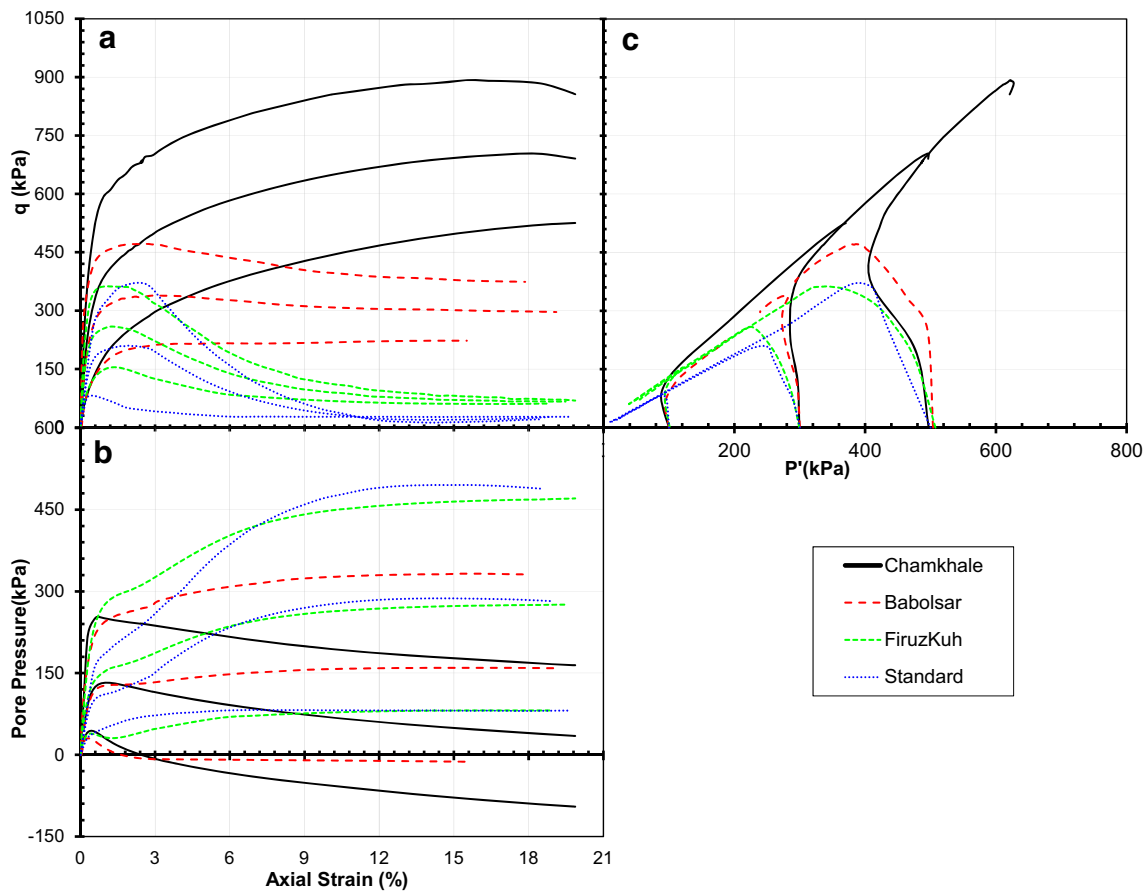
Fig. 10 Results of undrained triaxial tests **a** deviatoric stress versus axial strain, **b** excess pore water pressure versus axial strain, **c** stress path

indicate the tendency toward volume increase or decrease, the variations in pore water pressure with respect to axial strain have been calculated, and its maximum value is defined in this study as the "dilation tendency index", denoted by DT.

$$DT = -\left[\frac{dU}{d\varepsilon_a}\right]_{max} \qquad (8)$$

DT is calculated for all the tests, and the results are shown in the last column of Table 4. Similar to flow potential parameter, U_f, the Chamkhaleh sand has proven the highest tendency to dilation, under all consolidation stresses, while the Standard sand has compressed in all conditions. The DT has decreased with increase in consolidation stress in all sands.

6 Discussion

Triaxial compression tests have been carried out on four sand specimens with different particle shapes. The parameters relating to the shape of particles were calculated. The results of triaxial tests were also analyzed and

their parameters determined. The effects of particle shapes are evaluated on variations of parameters representing the behavior characteristics of each sand.

Figure 12 shows the variations of internal friction angle with the particle shape parameters. The best fit line and correlation coefficient are also plotted. As it may be seen, the use of roundness parameter is more suitable than the other parameters for estimation of the internal friction angle in these four sand types, as the range of roundness variations in the four studied sands is far more than the range of sphericity variations. The figure clearly indicates that with increase in roundness, the internal friction angle has decreased in peak and SS conditions. Chamkhaleh sand with the lowest roundness has exhibited the highest angle of internal friction. Cho et al. [18] proposed a linear correlation between roundness and large strain internal friction angle (Eq. 9) which is very close to the equation presented in Fig. 12b for SS condition (Eq. 10).

$$\phi = 42 - 17R \quad (\text{Cho et al. [18]}) \qquad (9)$$

$$\phi_{SSL} = 39.12 - 16.98R \quad (\text{This Study}) \qquad (10)$$

Variations of flow potential, U_f, and also dilation tendency index, DT, are presented and compared in Fig. 13.
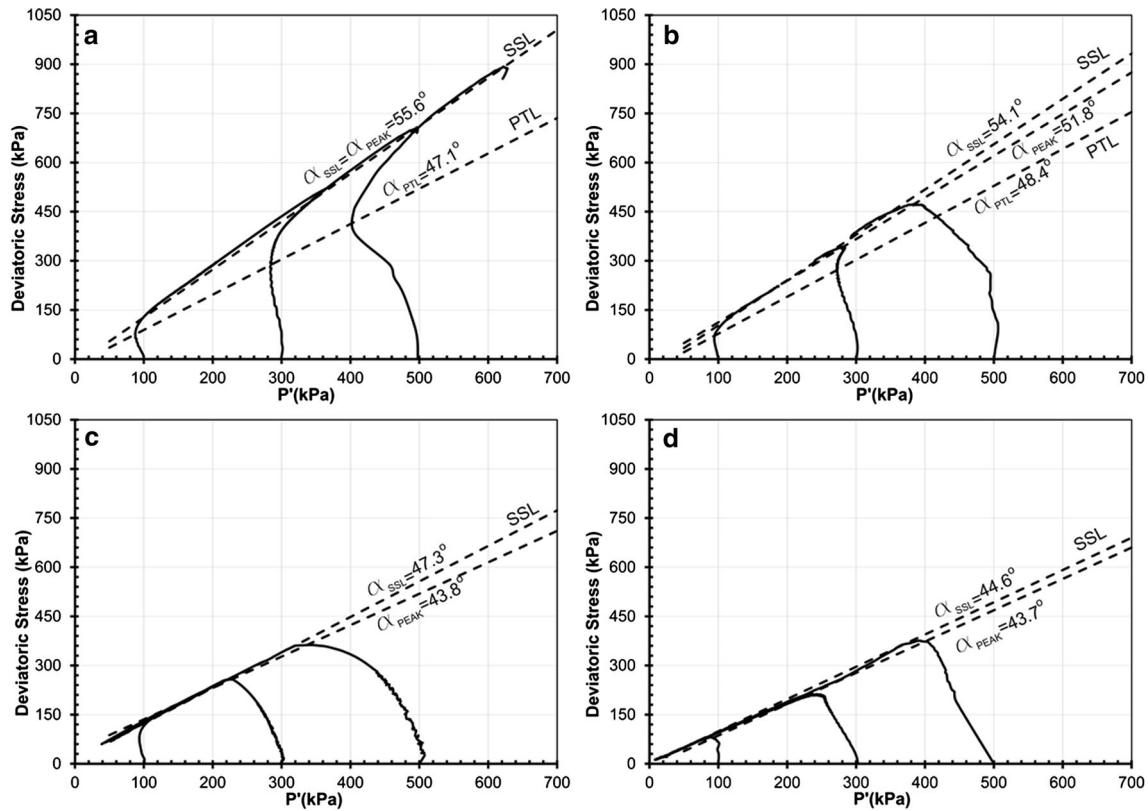
Fig. 11 Comparison of steady-state, maximum strength and phase transformation *lines* for **a** Chamkhaleh sand, **b** Babolsar sand, **c** Firouzkuh sand, and **d** Standard sand

Table 5 Comparison of the inclinations of the lines in the steady-state, maximum strength and phase transformation conditions

Sand	φ'_{SSL}	φ'_{peak}	α'_{SSL}	α'_{peak}	α'_{PT}
Chamkhale	36.0°	36.0°	55.6°	55.6	47.1°
Babolsar	34.2°	31.6°	54.1°	51.8°	48.4°
Firouzkuh	27.3°	24.4°	47.3°	43.8°	–
Standard	25.0°	24.4°	44.6°	43.7°	–

Similar to the previous diagram, the use of roundness is proved to be more suitable. Both U_f and tendency to contractive behavior increase with roundness and consolidation stress. It is worth noting that a sudden decrease in the slope of flow potential variations and tendency to dilation with roundness has occurred at an approximate roundness of 0.5. This figure also clearly demonstrates the highest tendency of the Chamkhaleh sand to dilation with lowest potential of static flow liquefaction.
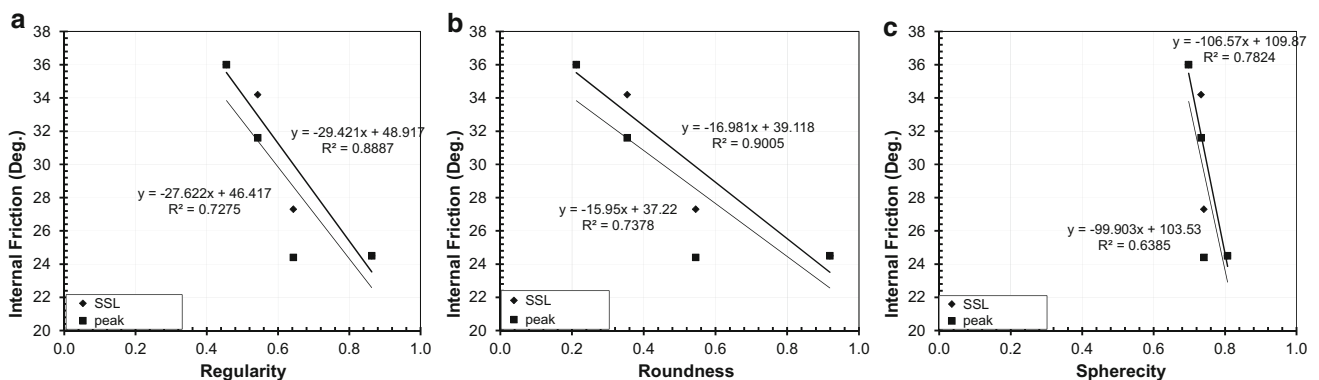

Fig. 12 Variations of internal friction angle with **a** regularity index, **b** roundness, and **c** sphericity

The image processing technique used in this study has shown that the sphericity of all the four sands is within a narrow band of 0.7 through 0.8. On the other hand, the wide range of roundness variations (0.2 through 0.92) has exhibited a clear relationship with all the dilative indices of the sands. Then, it can be stated that the distinct dilative response of Chamkhaleh sand with respect to the other sands is attributed to its lower roundness or, in fact, the high angularity of this sand. As the sphericity of the four sands is within a narrow band of 0.7–0.8, it cannot really be concluded that the effect of this shape parameter is insignificant. In fact, the increase of U_f and decrease of DT are evident in Fig. 13c, respectively, with sphericity, but another parameter that could have contributed to unusually high dilative tendency of Chamkhaleh sand is surface roughness or asperities of the surface of the grains. Reliable quantification of this parameter could not be made in this study.

7 Conclusions

Susceptibility to liquefaction depends on the initial state of sand with respect to the steady-state line in e-log p′ space; it is not common knowledge that the shape of particles affects the dilative behavior of sand so much that static liquefaction in loose sand in undrained conditions does not

occur at all (like in the case of Chamkhaleh sand). The parameters required for defining the shape of particles were quantified using the image processing method and MATLAB software for four sand types. Comparison of the results obtained from the image processing software and the presented diagram by Krumbein and Sloss [16] demonstrated the high precision of the utilized method in determination of roundness and sphericity criteria. On the other hand, more particles could be evaluated at a shorter period of time. The most important finding from the results of triaxial tests and shape parameter analyses are summarized below:

– The main factor contributing to very high tendency of Chamkhaleh sand to dilative response as compared to the other sands is the angularity of particles.
– Other than high tendency to dilation, the angle of internal friction of Chamkhaleh sand is higher than the other sands.
– A "dilation tendency index" parameter is introduced in this study, that can be used to quantify the tendency of sand specimens to dilative behavior in undrained tests.
– The internal friction angle at the steady-state condition is more dependent on the shape of particles than that at the maximum strength condition.
– Dependency of dilation tendency and flow potential parameters on roundness of particles for values less
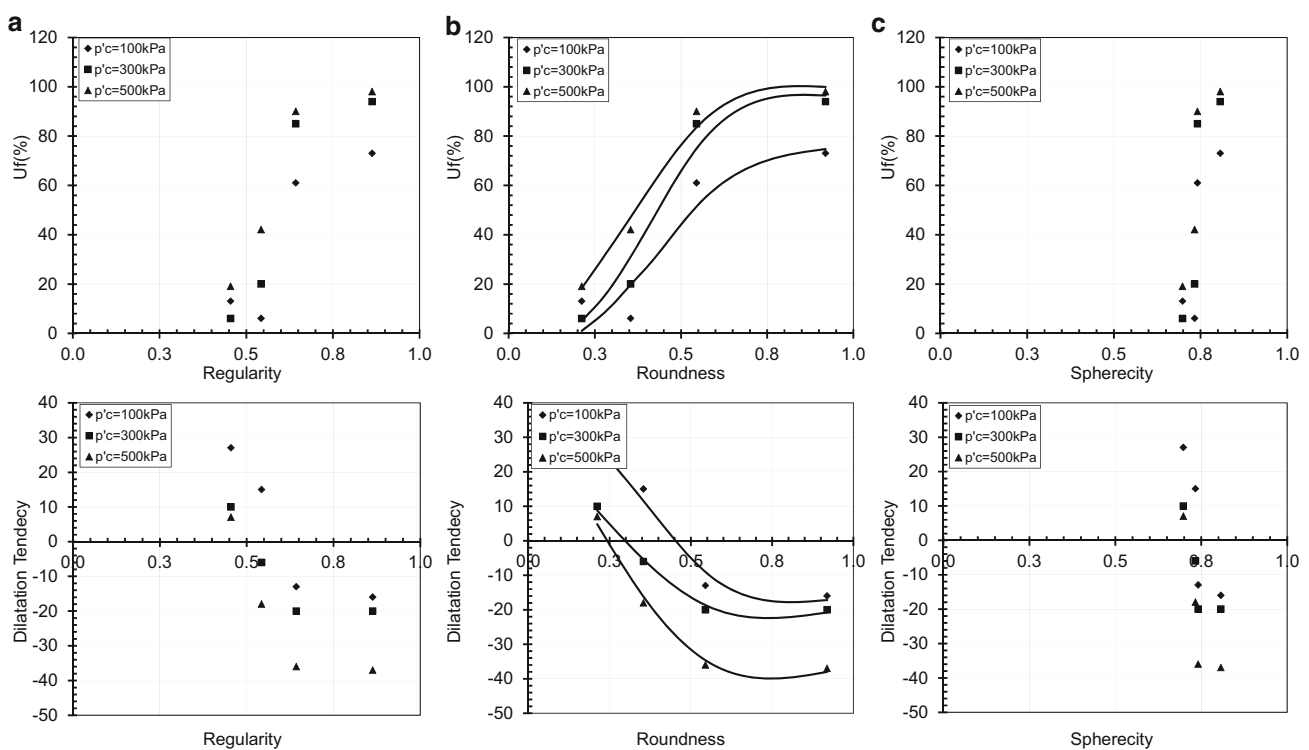

Fig. 13 Variations of flow potential and dilation tendency index with **a** regularity index, **b** roundness and **c** sphericity

than 0.5 is more than those of greater values. This dependency is reduced abruptly with an increase of roundness beyond 0.5.

– Using the regularity index, which was introduced by Choe et al. [18], is not suitable for cases in which the range of variations in either roundness or sphericity is limited, and hence, it is better to use parameters with a larger range of variations, such as roundness, in the present study.

References

1. Uthayakumar M, Vaid YP (1998) Static liquefaction of sands under multiaxial loading. Can Geotech Eng 35(2):273–283
2. Masayuki H, Hideyuki T, Noriyouki Y, Hidekazu M (1994) Undrained cyclic and monotonic triaxal behaviour of saturated loose sand. Soils Found 34(1):19–32
3. Santamarina JC, Cho GC (2004) Soil behaviour: the role of particle shape, Proceeding Skempton Conference, London
4. Castro G (1965) Liquefaction of sands, Ph.D Thesis, Harvard University, Cambridge
5. Casagrande A (1971) On liquefaction phenomena. Geotechnique 21(3):197–202
6. Lade PV (1975) Torsion shear tests on cohesionless soil. In: Proceeding Fifth Pan-American Conference on Soil Mechanics and Foundation Engineering 1, 117–127
7. Vaid YP, Chern JC (1985) Cyclic and monotonic undrained response of saturated sands. In: Proceeding Advances in the art of testing soils under cyclic conditions Conference, Detroit, p 120–147
8. Ishihara K (1993) Liquefaction and flow failure during earthquakes. Geotechnique 43(3):351–415
9. Yamamuro JA, Lade PV (1997) Static liquefaction of very loose sands. Can Geotech J 34(6):905–917
10. Riemer MF, Seed R (1997) B. factors affecting apparent position of the steady state line. ASCE J Geotech Eng 123(3):281–288
11. Yoshimine M, Ishihara K (1998) Flow potential of sand during liquefaction. Soils Found 38(3):189–198
12. Hassanlourad M, Rasouli MR, Salehzadeh H (2014) A comprasion between the undrained shear behavior of carbonate and quartz sands. Int J Civil Eng 12(4):338–350
13. Sadeghian S, Latifi Namin M (2013) Using State parameter to improve numerical prediction of a generalized plasticity constitutive model. Comput Geosci 51:255–268
14. Terzaghi K (1925) Principles of soil mechanics. Eng News Rec 5–832
15. Barret PJ (1980) The shape of rock particles, a critical review. Sedimentology 27:291–303
16. Krumbein WC, Sloss LL (1963) Stratigraphy and sedimentation, 2nd edn. W.H. Freeman and Company, San Francisco
17. Alshibli KA, Alsaleh MI (2004) Characterizing surface roughness and shape of sands using digital microscopy. ASCE J Comput Civil Eng, p 36–45
18. Cho GC, Dodds J, Santamarina JC (2006) Particle shape effects on packing density, stiffness, and strength: natural and crushed sands, ASCE J Geotech Geoenviron Eng, p 591–602
19. Al-Raoush R (2007) Microstructure characterization of granular materials. Physica 273:545–558
20. Cavarretta I (2009) The influence of particle characteristics on the engineering behaviour of granular materials, Ph.D Thesis, University Imperial College London, London
21. Shabani F (2009) Completion and start-up of simple shear apparatus and liquefaction assessment Chamkhaleh sand, M.Sc. Thesis, Department of Civil and Environmental engineering, AmirKabir University of Technology, Tehran
22. Kargar SHR, Shahnazari H, Salehzadeh H (2014) Post-cyclic behavior of carbonate sand whit anisotropic consolidation. Int J Civil Eng 12(4):316–325
23. ASTM C778 (2013) Standard specification for standard sand, American Society for Testing and Materials
24. Bahadori H, Ghalandarzadeh A (2008) Effect of non plastic silt on the anisotropic behavior of sand. Soils Found 48(4):531–545
25. Eghbali AH, Fakharian K (2014) Effect of principal stress rotation in cement-treated sands using triaxial and simple shear tests. Int J Civil Eng 12(1):1–14
26. Hashemi M (2013) Evaluation of engineering geological characteristics of Caspian Sea coast in Guilan Province with respect to geo-environmental hazards, Ph.D thesis, Tarbiat Modares University, Tehran
27. Kazanci N, Gulbabazadeh T, Suludere Y (2010) Geological evolution of the Sefidrud Delta, Southern Caspian Sea, Iran, International conference on Tectonic Crossroads: Evolving Orogens of Eurasia-Africa-Arabia. Middle East Technical University, Ankara, pp 4–8
28. Lahijani A, Rahimpour-Bonab H, Tavakoli V, Hosseindoost M (2009) Evidence for late Holocene highstands in Central Guilan-East Mazanderan, South Caspian coast, Iran. Quatern Int 197:55–71
29. Wadell H (1932) Volume, Shape and roundness of rock particles. J Geology 40:443–451
30. Masad E, Olcott D, White T, Tashman L (2001) Correlation of fine aggregate imaging shape indices with asphalt mixture performance, Transportation Research Record 1757. Transportation Research Board, Washington, DC, pp 148–156
31. Hyslip JP, Vallejo LE (1997) Fractal analysis of the roughness and size distribution of granular materials. Eng Geol 48:231–244
32. Bowman ET, Soga K (2001) Drummnond W Particle shape characterization using Fourier descriptor analysis. Géotechnique 51(6):545–554
33. Ladd RS (1978) Preparing test specimens using under compaction. Geotech Test J 1(1):16–23
34. Skempton AW (1954) Pore-pressure Coefficients A and B. Geotechnique 4(4):143–147
35. Lade PV (1977) Hernandes SB membrane penetration effects in undrained tests. J Geotech Eng Div 103(2):109–125
36. Bolton MD (1986) The strength and dilatancy of sands. Geotechnique 36(1):65–78
37. Vaid YP, Sasitharan S (1992) The strength and dilatancy of sand. Can Geotech J 29(3):522–526